Influences of subgrid scale dynamics on resolvable scale statistics in large-eddy simulations [1]

Thierry Dubois, François Jauberteau

Laboratoire de Mathématiques Appliquées, Université Blaise Pascal and CNRS (URA 1501)

63177 Aubière (France)

Ye Zhou

Institute for Computer Applications in Science and Engineering

NASA Langley Research Center, Hampton, VA 23681 (U.S.A.)

Abstract

Recently, the ϵ-expansion and recursive renormalization group (RNG) theories as well as approximation inertial manifolds (AIM) have been exploited as means of systematically modeling subgrid scales in large-eddy simulations (LES). Although these theoretical approaches are rather complicated mathematically, their key approximations can be investigated using direct numerical simulations (DNS). In fact, the differences among these theories can be traced to whether they retain or neglect interactions between the subgrid-subgrid and subgrid-resolvable scales. In this paper, we focus on the influence of these two interactions on the evolution of the resolvable scales in LES: the effect^A which keeps only the interactions between the small and large scales; and, the effect^B which, on the other hand, keeps only the interactions among the subgrid-subgrid scales. The performance of these models is analyzed using the velocity fields of the direct numerical simulations. Specifically, our comparison is based on the analysis of the energy and enstrophy spectra, as well as higher-order statistics of the velocity and velocity derivatives. We found that the energy spectrum and higher-order statistics for the simulations with the effect^A (referred to, hereafter, as model^A) are in very good agreement with the filtered DNS. The comparison between the computations with effect^B (referred to, hereafter, as model^B) and the filtered DNS, however, is not satisfactory. Moreover, the decorrelation between the filtered DNS and model^A is much slower than that of the filtered DNS and model^B. Therefore, we conclude that the model^A, taking into account the interactions between the subgrid and resolvable scales, is a faithful subgrid model for LES for the range of Reynolds numbers considered.

[1]This work was supported by the National Aeronautics and Space Administration under NASA Contract No. NAS1-19480 while two of the authors (Y. Z. and T. D.) were in residence at the Institute for Computer Applications in Science and Engineering (ICASE), NASA Langley Research Center, Hampton, VA 23681.

1. Introduction

Although direct numerical simulations (DNS) can be extremely useful in many areas related to the study of turbulence physics and the assessment of theories, it is restricted to relatively low Reynolds number (Re). Virtually all scientific and engineering calculations of nontrivial turbulent flows at high Re are based on some type of modeling.

Large-eddy simulation (LES) is a logical 'modeling extension' of DNS. LES is based on the observation that the small scales are more universal in character than the large energy containing scales of motion, that are primarily responsible for turbulent transport. LES is useful in the study of turbulence physics at high Reynolds numbers that are unattainable by DNS. LES is also intended to be useful in the development of turbulence models for the prediction of the complex flows of technical interest where simpler modeling approaches fail [1]. In LES, the three-dimensional time-dependent motion of these large scales are computed directly while the small scales are modeled (the so called 'subgrid scale modeling' problem; see [2] and [1]). Thus, the mechanism by which the subgrid modes remove energy from large scale modes must be compensated for; and this compensation is traditionally achieved by suitable enhancing the numerical value of the viscosity. However, it is well known that this type of eddy viscosity models suffers from a lack of phase information. The minimum requirement for a subgrid modeling is that, at the very least, the energy spectrum is preserved. Ideally, an LES field should be statistically the same as the large scales of a fully-resolved DNS, not withstanding the inaccuracy in the representation of the small scale by a subgrid model ([3]).

Recently, the renormalization group theory (RNG) and approximate inertial manifolds (AIM) have been applied to turbulence. The RNG methods fall into two distinct categories: (a) ϵ-RNG, pioneered by Forster *et al.* ([4]), and (b) recursive-RNG, pioneered by Rose ([5]). These techniques have been criticized and compared ([6]-[11]) Unfortunately, there is no systematical study of these theoretical approaches using direct numerical simulations. In this paper, we investigate the key approximations of these theories using DNS. In particular, our objective is to find out the influence

of the small scale dynamics on the energy spectrum and higher-order statistics of the resolvable scale evolution. This analysis leads to two interesting models.

2. Preliminary

Both the RNG and AIM approaches are iterative methods. However, for our purpose one needs only to examine the removal of the first subgrid scale shell from the Navier-Stokes equation. We denote k_1 as the cut-off wavenumber that separates the resolvable scales from the small scales and introduce the usual notation

$$u_\alpha(\mathbf{k},t) = \begin{cases} u_\alpha^>(\mathbf{k},t) & \text{if } k_1 < k < k_0, \\ u_\alpha^<(\mathbf{k},t) & \text{if } k < k_1, \end{cases}$$

where k_0 is greater than the Kolmogorov wavenumber, and k represents $|\mathbf{k}|$. For $k < k_1$, the resolvable scale Navier-Stokes equation is

$$\Big[\frac{\partial}{\partial t} + \nu_0 k^2\Big] u_\alpha^<(\mathbf{k},t) = M_{\alpha\beta\gamma}(k) \int d^3j [u_\beta^<(\mathbf{j},t) u_\gamma^<(\mathbf{k}-\mathbf{j},t)$$

$$+ \underbrace{2u_\beta^>(\mathbf{j},t) u_\gamma^<(\mathbf{k}-\mathbf{j},t)}_{A} + \underbrace{u_\beta^>(\mathbf{j},t) u_\gamma^>(\mathbf{k}-\mathbf{j},t)}_{B}], \tag{1}$$

where $M_{\alpha\beta\gamma}(k) = \frac{1}{2i}[k_\beta D_{\alpha\gamma}(k) + k_\gamma D_{\alpha\beta}(k)]$ and $D_{\alpha\beta}(k) = \delta_{\alpha\beta} - k_\alpha k_\beta / k^2$. For the subgrid scale, $k_1 < k < k_0$, we have

$$\Big[\frac{\partial}{\partial t} + \nu_0 k^2\Big] u_\alpha^>(\mathbf{k},t) = M_{\alpha\beta\gamma}(k) \int d^3j [\underbrace{u_\beta^<(\mathbf{j},t) u_\gamma^<(\mathbf{k}-\mathbf{j},t)}_{I}$$

$$+ \underbrace{2u_\beta^>(\mathbf{j},t) u_\gamma^<(\mathbf{k}-\mathbf{j},t)}_{II} + \underbrace{u_\beta^>(\mathbf{j},t) u_\gamma^>(\mathbf{k}-\mathbf{j},t)}_{III}]. \tag{2}$$

Equations (1) and (2) are very different since the wavenumber $\mathbf{k}$ is in the resolvable and subgrid scales, respectively. All three methods omit term (III) of the subgrid dynamical equation since it is very small. Note that the comparable term (B) in equation (1) is not negligible.

One solves the small scales equation (2), and then substitutes it into the corresponding resolvable scale equation. During the process, the ϵ-RNG and AIM procedures make several approximations

to (1) and (2).

2.1. ϵ-Renormalization group

In ϵ-RNG ([12]–[14]), one invariably introduces a zero-mean Gaussian random forcing term into the Navier-Stokes equation. This white noise forcing is determined by its correlation function, which is assumed to obey a subgrid wavenumber power-law spectrum. A small parameter ϵ is introduced into the exponent of this power-law. The method of ϵ-expansion has been discussed in detail by Kraichnan in [6].

Regardless of the details of the argument, the net effect of the ϵ-RNG is to neglect term (A) of (1) and term (I) of (2). Therefore, the dynamics of subgrid scales in the resolvable scale equation is reflected only in an approximated form of the term (B) in (1)

$$\Big[\frac{\partial}{\partial t}+\nu_0 k^2\Big]u_\alpha^<(\mathbf{k},t)=M_{\alpha\beta\gamma}(k)\int d^3j[u_\beta^<(\mathbf{j},t)u_\gamma^<(\mathbf{k}-\mathbf{j},t)+\underbrace{u_\beta^>(\mathbf{j},t)u_\gamma^>(\mathbf{k}-\mathbf{j},t)}_{B}], \tag{3}$$

and for the subgrid scale, $k_1<k<k_0$,

$$\Big[\frac{\partial}{\partial t}+\nu_0 k^2\Big]u_\alpha^>(\mathbf{k},t)=M_{\alpha\beta\gamma}(k)\int d^3j[\underbrace{2u_\beta^>(\mathbf{j},t)u_\gamma^<(\mathbf{k}-\mathbf{j},t)}_{II}]. \tag{4}$$

One calculates the effect of removing a small wavenumber shell on the Navier-Stokes equation. One of the resulting effects is that the molecular viscosity is replaced by a turbulent viscosity. It is the outcome after substituting the formal solution of (4) into term-B in the resolvable scale equation (1). Furthermore, the distant interaction approximation, $k\to 0$, is taken which effectively introduces a spectral gap between the subgrid and resolvable scales.

The formal solution of (2) has two contributions. We have considered the effect of the term (II) above. Another effect from term (I) is the introduction of triple nonlinearities into the renormalized equation. To recover the Kolmogorov energy spectrum, one must choose $\epsilon=4$ while assuming that the triple nonlinearities can be neglected [12]. Recently, Eyink [15] has claimed that this argument is flawed.

2.2. Recursive renormalization group

The recursive RNG ([16]-[19]) has been developed and applied to subgrid scale modeling of Navier-Stokes turbulence. The major differences between the two RNG procedures are that in the recursive RNG:

- the ϵ-expansion is not applied,
- the turbulent transport coefficients are determined for the whole range of resolvable wavenumber scales (with given small scale velocity correlation function), and
- triple nonlinearities are generated and retained in the renormalized Navier-Stokes equation.

2.3. Approximate inertial manifolds

In the AIM theory advanced by Foias, Manley, and Teman, ([20], [21]; referred to, hereafter, as FMT), the evolution equation for the resolvable scale is approximated to

$$\Big[\frac{\partial}{\partial t}+\nu_0 k^2\Big]u_\alpha^<(\mathbf{k},t)=M_{\alpha\beta\gamma}(k)\int d^3j[u_\beta^<(\mathbf{j},t)u_\gamma^<(\mathbf{k}-\mathbf{j},t)+\underbrace{2u_\beta^>(\mathbf{j},t)u_\gamma^<(\mathbf{k}-\mathbf{j},t)}_{A}], \tag{5}$$

while for the subgrid scale, $k_1<k<k_0$,

$$\Big[\frac{\partial}{\partial t}+\nu_0 k^2\Big]u_\alpha^>(\mathbf{k},t)=M_{\alpha\beta\gamma}(k)\int d^3j[\underbrace{u_\beta^<(\mathbf{j},t)u_\gamma^<(\mathbf{k}-\mathbf{j},t)}_{I}+\underbrace{2u_\beta^>(\mathbf{j},t)u_\gamma^<(\mathbf{k}-\mathbf{j},t)}_{II}]. \tag{6}$$

In mathematical language of AIM, inertial manifolds provide an interaction law between the small and large scales of a flow. Following Kraichnan, FMT balanced the $\frac{\partial \mathbf{u}^>}{\partial t}$ with the term-II in (6). As a result, the subgrid velocity modes are slaved to the resolvable scale ones

$$\nu_0 k^2 u_\alpha^>(\mathbf{k},t)=M_{\alpha\beta\gamma}(k)\int d^3j[u_\beta^<(\mathbf{j},t)u_\gamma^<(\mathbf{k}-\mathbf{j},t)]. \tag{7}$$

At each step, FMT invoked some inequalities, which bound the appropriate norms of the solutions to the Navier-Stokes equations. This procedure leads to a modification of the momentum equation,

viz the introduction of the triple nonlinear term. The resulting iterative procedure does not invoke any statistical properties of the solutions of Navier-Stokes equations, since the interactions between small scales, the term-B in (1), are omitted. Such a term can be rewritten into the enhanced eddy viscosity by constructing an equation for the second moments.

Several numerical schemes related to AIM have been proposed. In these schemes, different levels are defined by projecting the flow into the small and large scales, which are then treated differently using the time multilevel methods. Such numerical schemes lead to a model for the cross interaction as well for the subgrid-subgrid interaction terms and the reader is referred to [22], [23], and the references therein for details. For the latest developments in numerical computation, see recent papers [24]–[26] in special issue of *Theoret. Comp. Fluid Dynamics*: "Inertial manifolds and their application to the simulation of turbulence" [27].

3. Numerical experiments and simulated isotropic DNS flow fields

3.1. Description of the DNS

The spatial discretization of (1) and (2) was achieved by a Fourier Galerkin method, where the truncated nonlinear terms were computed by pseudo-spectral method. For time integration, we used an exponential propagation of the linear part, which leads to an exact integration, and a Runge-Kutta scheme of third order for the right-hand side (RHS) of the equations (1)-(2). For a detailed description of the schemes and of the resolved equations, the reader is referred to [22] and [26].

3.2. Description of the models

To investigate the influence of the nonlinear interaction terms (A) and (B) on the time evolution of the resolvable scales $u_\alpha^<(\mathbf{k})$, we have implemented two models. In the first method, named model^A, we compute $u_\alpha^{<,A}(\mathbf{k},t)$ with the equation (1) in which the term (B) is neglected:

$$\Big[\frac{\partial}{\partial t}+\nu_0 k^2\Big]u_\alpha^{<,A}(\mathbf{k},t)=M_{\alpha\beta\gamma}(k)\int d^3j[u_\beta^{<,A}(\mathbf{j},t)u_\gamma^{<,A}(\mathbf{k}-\mathbf{j},t)+2u_\beta^{>,DNS}(\mathbf{j},t)u_\gamma^{<,A}(\mathbf{k}-\mathbf{j},t)]. \quad (8)$$

Here, $\mathbf{u}^{>,DNS}$ corresponds to the small scales of the DNS velocity field $\mathbf{u}^{DNS}$ that is obtained by solving the full system (1), (2) without making any approximation regarding the nonlinear terms (see [28] for a preliminary attempt to examine the effects of the cross interactions).

For the second method, named model^B, we evaluate $u_\alpha^{<,B}(\mathbf{k},t)$ with the equation (1) in which the term (A) is neglected:

$$\Big[\frac{\partial}{\partial t}+\nu_0 k^2\Big]u_\alpha^{<,B}(\mathbf{k},t)=M_{\alpha\beta\gamma}(k)\int d^3j[u_\beta^{<,B}(\mathbf{j},t)u_\gamma^{<,B}(\mathbf{k}-\mathbf{j},t)+u_\beta^{>,DNS}(\mathbf{j},t)u_\gamma^{>,DNS}(\mathbf{k}-\mathbf{j},t)]. \quad (9)$$

These two models can be summarized as following. The model^A model keeps only the cross interactions between the resolvable and subgrid scales while neglecting the influence of the interaction among small scales on the evolution of the large ones. The model^B, on the other hand, keeps the subgrid interaction term, while neglecting the interactions between the subgrid-resolvable scales.

As it was pointed out before, the "modeled LES" fields should be statistically the same as the large scales of the DNS field. Hence, in order to check the validity of the model^A and model^B, the solutions $u_\alpha^{<,A}$ and $u_\alpha^{<,B}$ are compared with $u_\alpha^{<,DNS}$, the filtered DNS solution (fDNS).

3.3. Comparison of the LES models with filtered DNS

For the sake of completeness, we compare the models with the filtered DNS on several aspects. The proper resolution of the resolvable scales and the resolution of the energy transfers can be checked by evaluating the energy spectrum of the velocity field

$$E(k,t)=\frac{1}{2}\sum_{|\mathbf{k}|\in[k-\frac{1}{2};k+\frac{1}{2})}|\mathbf{u}(\mathbf{k},t)|^2. \quad (10)$$

Since turbulence is isotropic, we have averaged over the spheric shell centered at k. Also the higher-order moments of the distributions of a velocity component u_1 and its longitudinal and transverse gradients $\left(\frac{\partial u_1}{\partial x_1}\right)$ and $\left(\frac{\partial u_1}{\partial x_2}\right)$ are computed. The nth-order flatness, denoted as F_n, is given by

$$F_n(v) \;=\; (-1)^n\frac{\langle v^n\rangle}{\langle v^2\rangle^{\frac{n}{2}}}, \quad (11)$$

where $\langle - \rangle$ denotes an ensemble average which corresponds to a volume average over the whole domain. These quantities are important characteristics of turbulent flows. In particular, F_3 and F_4 are the well known skewness and flatness factors, respectively. The skewness factor of the longitudinal derivative of velocity has been found to be independent of the Reynolds number and is strongly associated with the inertial range scales. For a fully developed turbulent flow, $F_3(\frac{\partial u_1}{\partial x_1})$ should be of the order of 0.5. The flatness factor of the longitudinal derivative of velocity is an increasing function of the Reynolds number and is strongly associated with the dissipation range scales.

Finally, a correlation coefficient between the filtered DNS and the LES fields (as in [3]) is evaluated

$$\Gamma \;=\; \frac{\langle \mathbf{u}.\mathbf{u}' \rangle}{\langle \mathbf{u}^2 \rangle^{\frac{1}{2}} \langle \mathbf{u}'^2 \rangle^{\frac{1}{2}}}. \tag{12}$$

This coefficient Γ $(-1 \leq \Gamma \leq 1)$ estimates the statistical independence of the fields $\mathbf{u}$ and $\mathbf{u}'$ and is a function of the time t. For two velocity fields that are identical in the large scales but different in the small scales, Leith and Kraichnan (cf. [29]) found that they will become decorrelated after one eddy turnover time. Hence by computing the coefficient Γ, we can measure how faithfully these two models represent the filtered DNS.

3.4. Simulated flow fields

In next section, we present the results obtained with two simulations referred as S_1 and S_2 hereafter.

Statistical steady state: S_1

As initial condition, we use the result from a 96^3 simulation, which has reached a statistically steady state after integrating over $8,000$ time iterations. We consider that a flow becomes statistically steady when the time average of all its quantities (energy, enstrophy, spectrum, higher-order moments, ...) are nearly time independent. Here, the resolution of the simulation is 128^3 so that the highest resolved wavenumber is $k_0 = 64$. The time integration has been conducted over 27

Table 1 : Characteristic parameters of the simulations S_1 and S_2. We denote by k_F the wavenumber of the external force and T is the final time of the integration.

	Re_λ	k_η	$\frac{k_0}{k_\eta}$	$\frac{k_1}{k_\eta}$	$\frac{T}{\tau}$	k_F
S_1	70	30	2	0.5	27	1
S_2	70	53	1.2	0.3	12	2

eddy turnover times[2]. The Taylor microscale Reynolds number Re_λ is of the order of 70 for this simulation. The Kolmogorov (dissipation) wavenumber k_η was around 30 so that $k_0/k_\eta \simeq 2$. Here, k_η is defined as usually y $k_\eta = \left(\frac{\varepsilon_r}{\nu^3}\right)^{\frac{1}{4}}$ and $\varepsilon_r = 2\nu \int_0^{+\infty} k^2 E(k) dk$ is the energy dissipation rate. These values have been time averaged over the interval $[0, 27\tau]$. The cut-off wavenumber k_1 was chosen equal to 16, so that k_1/k_η is of the order of 0.5. With the choice of these parameters, the simulation S_1 is similar to the one described in [3].

The forcing term used is time independent and similar to the one used in [23]. In order to obtain an inertial range sufficiently extended for such spatial resolution, the energy injection rate acts on the lowest modes $\mathbf{u}(\mathbf{k}, t)$ with $|\mathbf{k}| = k_F = 1$.

Perturbation of a random initial field: S_2

The major difference between S_2 and S_1 is the initial condition. Here, we imposed a spectrum

$$E_0(k) = c_0 \; k^4 \; e^{-\left(\frac{k}{k_2}\right)^2} \tag{13}$$

where $k_2 = 4$, instead of an initial $k^{-\frac{5}{3}}$ spectrum in S_1. The external force is of the same type as for S_1 but k_F was set to 2 instead of 1. The Reynolds number is of the same order i.e. $Re_\lambda \sim 70$. As a result of these choices, the Kolmogorov wavenumber is larger, see Table 1 which summarizes the characteristic parameters for both simulations, so that the small (DNS) scales for $k > k_1$ contain more energy than in the previous simulation.

[2]The eddy turnover time τ is defined as $\tau = \frac{L}{U}$ where $U = \left\langle |\mathbf{u}|^2 \right\rangle^{1/2}$ is a characteristic velocity and $L = \frac{\int_0^{+\infty} k^{-1} E(k) dk}{\int_0^{+\infty} E(k) dk}$ is an integral scale.

4. Results

4.1 The velocity spectra

We first consider the results of simulation S_1. Figure (1a) shows the energy and enstrophy spectra corresponding to DNS, model^A and model^B at the intermediate time $t = 13.5\tau$. It is clear that the model^A provides a better resolution of the resolvable scale energy spectrum. A departure of the model^A spectrum from the fDNS spectrum can be noted near the cut-off, however there is no time amplification (see Figure 1b showing the spectra at the final stage of the simulation $T = 27\tau$). We note that an energy pile-up appears near the cut-off wavenumber k_1 on the model^B spectrum. This amount of energy, which is not dissipated, tends to accumulate and to modify the slope of the spectrum for $k < k_1$, even on short time integration. A such phenomenon does not appear on the model^A spectrum. Hence, by taking into account the cross interaction term (A), a better description of the energy transfers is achieved.

We now turn our attention to simulation S_2. Figures (1c) and (1d) illustrate the energy and enstrophy spectra at the intermediate time $t = 6\tau$ and at the final integration time $T = 12\tau$, respectively. At the intermediate time, we note that the model^A spectrum and the DNS spectrum are very close, while the model^B spectrum exhibits a modified slope. As in the previous simulation, an energy pile-up near the cut-off wavenumber appears on the model^B spectrum.

Figure (1d) reveals the limitation of the model^A at an extended simulation. We find that after 12 eddy turnover times, an energy pile-up also appears. Indeed, the accumulation of energy near the cut-off separation k_1 perturbs the energy spectrum leading to the departure from the Kolmogorov $k^{-\frac{5}{3}}$ inertial range scaling. Some improvement can be achieved by using an adaptive procedure to choose the cut-off wavenumber k_1 between $\mathbf{u}^<$ and $\mathbf{u}^>$ (see, for example, [23] and [26]).

It is interesting to note that for simulation S_1, the curves of the model^A and fDNS spectra remain close to each other even after 27 eddy turnover times. This can be explained by the fact that the initial condition chosen for S_2 induced strong perturbations during the transition period (indeed

$k_0/k_\eta \simeq 1.2$ for S_2 while $k_0/k_\eta \simeq 2.0$ for S_1), leading to different behaviors of the energy transfer terms to achieve the equilibrium state. The reader is referred to Sec. 5 for additional discussion. Time averaged compensated energy spectra of simulations S_1 and S_2 are presented on Figures 2.

4.2. The higher-order statistics

For the range of the Reynolds number Re_λ considered, the results of the DNS are in agreement with the DNS results obtained by Jimenez *et al.* in [33]. In Tables 2 and 3, we present the higher-order statistics of the velocity and of the velocity derivative for S_1 and S_2, respectively. In Table 2, the values listed were time averaged over the time interval $(0, 27\tau)$ while in Table 3, the quantities have been averaged over the time interval $(0, 3\tau)$.

First, as it was noted in [3], the fDNS values are more Gaussian than the values obtained from the full DNS. This is a consequence of the lack of the small scales. When estimating the moments of the filtered DNS, one does not take into account the intermittency phenomena. By comparing the values of the moments $F_n(\frac{\partial u_1}{\partial x_j})$ reported in Table 2, we find that the resolvable scale velocity field from the model^A has rather similar statistics as that of the fDNS. In contrast, the resolvable scale velocity field from the model^B has a tendency to be more Gaussian than the DNS and fDNS velocity fields. This is particularly evident on the moments of odd order. These results are confirmed by examining the higher-order statistics of S_2 (Table 3): the higher-order statistics of the velocity derivative estimated with model^B tends to be more Gaussian than the model^A field, which exhibits the same statistics as the fDNS field.

We now consider the time evolution of the skewness and flatness $F_n(\frac{\partial u_1}{\partial x_1}), n = 3, 4$ (cf. Figures 3 and 4) and of the flatness $F_4(u_1)$ (cf. Figures 5). For the simulation S_1, we note that the skewness obtained by the model^A and model^B have different behavior and different order of magnitude (Figure 3a), whereas the flatness remain close to each other at the same order of magnitude (Figure 4a). It appears that the odd order moments depend heavily on the inertial range (resolvable scales), whereas the even order moments strongly depend on the dissipative range (subgrid scales). Indeed,

Table 2 : Higher-order moments of the velocity component u_1 and its longitudinal and transverse gradients $\frac{\partial u_1}{\partial x_1}$ and $\frac{\partial u_1}{\partial x_2}$. The values for a Gaussian field are listed for comparison.

	u_1		$\frac{\partial u_1}{\partial x_1}$				$\frac{\partial u_1}{\partial x_2}$	
	F_4	F_6	F_3	F_4	F_5	F_6	F_4	F_6
Gaussian			0.0	3.0	0.0	15.0		
DNS	2.63	10.62	0.48	4.91	8.36	65.49	6.99	153.56
fDNS	2.63	10.52	0.40	4.09	5.18	36.78	5.34	69.45
Model^A	2.63	10.53	0.37	4.16	5.20	38.56	4.78	56.05
Model^B	2.55	9.88	0.24	4.03	3.60	36.16	4.35	42.05

as the fDNS, model^A and model^B compute only a part of the inertial range of the DNS spectrum ($k_1/k_\eta = 0.5$), the values of the odd moments are directly affected while the even moments are not. The model^A shows an improved performance over that of model^B on the time evolution of the flatness factor of velocity (Figure 5a). For the simulation S_2 ($k_1/k_\eta = 0.3$), Figures 3b, 4b and 5b show the time evolution of the skewness and flatness corresponding to $\frac{\partial u_1}{\partial x_1}$ and u_1. Their behaviors are similar to that of S_1. The velocity derivative skewness corresponding to the model^B decreases to zero after less than one eddy turnover time, whereas the one corresponding to the model^A remains close to the fDNS skewness until much later time. The change in skewness at $t = 6\tau$ is consistent with the behavior of the energy spectrum shown in Section 4.1. Furthermore, the model^A shows a better performance over the model^B on both the flatness factor of velocity derivative (Figure 4b) and velocity (Figure 5b).

The focus of Shtilman and Chasnov's work [3] was on the higher-order statistics. They found that the statistics of their LES model are in good agreement with the filtered DNS field. Indeed,

Table 3 : Higher-order statistics of the DNS, the filtered DNS and both LES fields.

	u_1	$\frac{\partial u_1}{\partial x_1}$	
	F_4	F_3	F_4
Gaussian		0.0	3.0
DNS	2.96	0.54	4.60
fDNS	2.94	0.43	3.57
Model^A	2.94	0.44	3.59
Model^B	2.99	0.13	3.44

their DNS, filtered DNS, and LES results on the higher-order statistics are very close to the present results.

4.3. Correlation coefficient

Figure 6 shows the time evolution of the correlation coefficient, defined in (12), for the simulation S_1. As time increases, the correlation coefficient between the fDNS and model^B decreases more rapidly than that between the fDNS and model^A. After 10 eddy turnover times, the model^A coefficient remains of the order of 1, while the model^B coefficient is close to 0.75. After this period (i.e. for $t > 10\tau$), both coefficients have a similar behavior and decay as $t/3$, before reaching a short plateau. This result shows the importance of the cross-interaction term (A) in subgrid modeling: the cross interaction term provides not only the correct magnitude for the energy, but also the phase information from the subgrid scale.

In [3], the correlation coefficient Γ decays faster to zero: the LES and fDNS fields become independent after two eddy turnover times. The measured values of Γ here decrease much slower since

the models investigated in this paper are more accurate. Indeed, in both model^A and model^B, a part of the interaction terms is kept and computed directly with the small scales $\mathbf{u}^{>,DNS}$ of the full DNS. As a result, the velocity fields $\mathbf{u}^{<,A}$ and $\mathbf{u}^{<,B}$ remain correlated with $\mathbf{u}^{<,DNS}$ over a longer period of time than the one obtained in [3].

5. Discussion

In [3], Shtilman and Chasnov compared the statistics of the filtered DNS and a LES performed with the eddy viscosity obtained by adjusting instantaneously the energy spectrum of the LES to that of the DNS. Therefore, the agreement between the energy spectrum in filtered DNS and LES in their case is by construction. This should compare with present study where the energy spectrum is preserved by taking into account the cross interactions explicitly (the model^A). In a short note, Hossain ([28]) looked at the effect of the cross interaction term on the energy spectrum. He observed that the cross interaction term plays an important role in maintaining the resolvable scale energy spectrum near the cutoff wavenumber. However, his computation was done only at 32^3 and 64^3 resolutions. Furthermore, he did not study the effects of these cross interactions on the higher-order statistics.

Our results confirmed and further advanced the work by Zhou and Vahala ([18]) who examined individual contributions to the energy transfer equation constructed from (1), namely

$$\Big[\frac{\partial}{\partial t} + 2\nu_0 k^2\Big] E(k,t) = T^{<<}(k) + T^{><}(k) + T^{>>}(k), \tag{14}$$

with $k < k_1$. $T^{<<}(k)$ gives the rate of energy transfer to mode k from interactions between the resolvable scale velocity fields; $T^{><}(k)$ is the energy transfer rate to mode k from the interactions between resolvable scale and small scale modes; and $T^{>>}(k)$ is the transfer rate to mode k from the interactions between small scale modes. Using LES and DNS data sets, Zhou and Vahala found that $T^{<<}(k)$ moves the energy to higher resolvable scale wavenumbers – essentially to the last octave.

$T^{>>}(k)$ removes energy throughout the resolvable scales in a manner consistent with the concept of eddy viscosity. The term $T^{><}(k)$, on the other hand, removes energy from the last octave of the resolvable scales which was transferred there by $T^{<<}(k)$ ([18]). Therefore, $T^{><}(k)$ and $T^{>>}(k)$ correspond to the energy transfer due to local and nonlocal interactions, respectively. A detailed study of locality of energy transfer and interactions in isotropic turbulence can be found in [30]-[32]. Near k_1, $T^{><}(k)$ prevails upon $T^{>>}(k)$; hence when $T^{><}(k)$ is neglected in the equations, as it is done in model^B, the energy transferred by $T^{<<}(k)$ tends to accumulate for k near k_1, leading to an energy pile-up on $E(k,t)$.

Hence, in agreement with [18], we found that the role of the cross interaction term in the evolution of the resolvable scales can be summarized as follows:

- maintaining an energy balance,
- incorporating both local and nonlocal interactions,
- maintaining the Kolmogorov spectrum for the whole range of resolvable scales, and
- preserving the higher-order statistics (see discussion below).

We expect the cross interactions will remain an important contribution even at high Reynolds numbers.

As shown in Zhou and Vahala [18], the energy transfer due to interactions among subgrid scales (effect^B)is the only contributor to the spectral eddy viscosity for $k \in [0, k_c/2]$. At the moderate Reynolds number here, we have demonstrated that the influence of effect^B on resolvable scale statistics are rather limited. However, at high Reynolds numbers, we expect that the effect^B will become more important. The modeling of this effect, however, is relatively easy since it is purely dissipative [18].

When the effect of the large-scale velocity fields is very strong, the rapid distortion theory (RDT)[34]-[36] is a satisfactory linear theory to describes the short time behavior of the flow. Since the effect of the interactions among subgrid scales is weak in S1, the excellent agreement between our model^A and fDNS may be interpreted using the language of RDT. Indeed, the term of the effect^A, $u^> u^<$, can be argued as a linear one in terms of $u^<$ from the point of view of the evolution equation for the resolvable scales. The situation in S2 is different. In this case, the strength of the nonlinear term (interactions among subgrid scales) changes from weak to strong at about six eddy-turn-over time scale τ (see Figures (1c) and (1d)). This may offer an explanation for the excellent performance of the model^A at $t = 6\tau$ but its relatively poor agreement with fDNS at $t = 12\tau$.

6. Conclusions

Using direct numerical simulations, we have studied the major approximations of RNG and AIM approaches. In fact, the differences among these mathematically complicated theories can be traced to whether they keep or neglect interactions between the subgrid-subgrid and subgrid-resolvable scales. In this paper, we have paid special attention to the influence of these two interactions on the evolution of the resolvable scales. Along the way, our analysis leads to two "LES models": first, the model^A which only keeps the interactions between the subgrid and resolvable scales; second, the model^B which only keeps the interactions between the subgrid-subgrid scales. We have tested the performance of these models using the velocity fields from DNS. Specifically, we have compared the energy and enstrophy spectra, as well as higher-order statistics of the velocity and velocity derivatives. We found that the energy spectrum and higher-order statistics of the model^A are in very good agreement with the filtered DNS. However, the comparison between the model^B and the filtered DNS is not satisfactory. Finally, the decorrelation between the filtered DNS and model^A is much slower than that of the filtered DNS and model^B. We conclude that the model^A, taking into account the interactions between the subgrid and resolvable scales, is a faithful subgrid model

for LES at moderate Reynolds number. We expect that the effect^B will become more important at higher Reynolds number. However, the modeling of this interaction is relatively easy since it is purely dissipative.

Acknowledgments

T. Dubois wishes to express his thanks to Dr. Y. Hussaini who gives him the opportunity to visit ICASE and to perform this work in collaboration with Y. Zhou. The authors also thank Dr. S. Girimaji for several useful remarks.

The computations presented in this paper were performed on the Cray C90 (8 processors) of IDRIS (supercomputing center of CNRS located at Orsay, FRANCE).

References

[1] W.C. Reynolds (1990), *The potential and limitations of direct and large-eddy simulations,* in Whither Turbulence, edited by J. Lumley, Springer, Berlin, 313.

[2] R.S. Rogallo and P. Moin (1984), *Numerical simulation of turbulent flows*, Annu. Rev. Fluid Mech. **16**, 99.

[3] L. Shtilman and J.R. Chasnov (1992), *LES versus DNS: a comparative study*, Center for Turbulence Research, Proceedings of the Summer Program.

[4] D. Forster, D. Nelson and M. Stephen (1977), *Long-time tails and the large-eddy behavior of a randomly stirred fluid,* Physical Review A, **16**, 732.

[5] H.A. Rose (1977), *Eddy diffusivity, eddy noise and subgrid-scale modeling*, J. Fluid Mech. **81**, 719.

[6] R.H. Kraichnan (1987), *An interpretation of the Yakhot-Orszag turbulence theory,* Phys. Fluids **30**, 2400.

[7] L. Smith and W.C. Reynolds (1991), *On the Yakhot-Orszag renormalization group method for deriving turbulence statistics and models,* Phys. Fluids A, **4**, 364.

[8] S.H. Lam (1992), *On the RNG theory of turbulence,* Phys. Fluids A, **4**, 1007.

[9] Y. Zhou and G. Vahala (1992), *Local interactions in renormalization methods for Navier-Stokes turbulence,* Phys. Rev. A, **46**, 1136.

[10] Y. Zhou, G. Vahala, W.D. McComb and S.H. Lam (1993), *RNG for CFD? An Assessment of Current RNG Theories of Turbulence*, in 'Transition, turbulence, and combustion', edited by M.Y. Hussaini et al., Kluwer.

[11] Y. Zhou and C.G. Speziale (1993), *An Overview of RNG Methods in Turbulence Modeling: Panel Discussion Summary*, in 'Transition, turbulence and combustion', edited by M.Y. Hussaini et al., Kluwer.

[12] V. Yakhot and S.A. Orszag (1986), *Renormalization group analysis of turbulence. I. Basic theory*, Journal of Scientific Computing, **1**, 3-55.

[13] V. Yakhot and L.M. Smith (1992), *The renormalization group, the ϵ-expansion and derivation of turbulence models*, Journal of Scientific Computing, **7**, 35-61.

[14] W.P. Dannevik, V. Yakhot and S.A. Orszag (1987), *Analytical theories of turbulence and the ϵ-expansion,* Phys. Fluids, **30**, 2021.

[15] G. Eyink (1994), *The renormalization group method in statistical hydrodynamics*, Phys. Fluids, **6**, 3063.

[16] Y. Zhou, G. Vahala and M. Hossain (1988), *Renormalization group theory for the eddy viscosity in subgrid modeling*, Physical Review A, **37**, 2590-2598.

[17] Y. Zhou, G. Vahala and M. Hossain (1989), *Renormalized eddy viscosity and Kolmogorov's constant in forced Navier-Stokes turbulence*, Physical Review A, **40**, 5865-5874.

[18] Y. Zhou and G. Vahala (1993), *Reformulation of recursive-renormalization-group-based subgrid modeling of turbulence*, Physical Review E, **47**, 2503-2519.

[19] Y. Zhou and G. Vahala (1993), *Renormalization group estimates of transport coefficients in the advection of a passive scalar by incompressible turbulence,* Physical Review E, **48**, 4387.

[20] C. Foias, O. Manley and R. Temam (1988), *Modeling on the interaction of small and large eddies in two dimensional turbulent flows*, M^2AN, **22**, 93-114.

[21] C. Foias, O. Manley and R. Temam (1991), *Approximate inertial manifolds and effective viscosity in turbulent flows*, Phys. Fluids A, **3**, 898-911.

[22] T. Dubois, F. Jauberteau and R. Temam (1993), *Solution of the incompressible Navier-Stokes equations by the Nonlinear Galerkin method*, Journal of Scientific Computing, **8**, 167-194.

[23] T. Dubois and F. Jauberteau (1995), *A dynamic multilevel model for the simulation of the small structures in homogeneous isotropic turbulence*, personal communication.

[24] M.S. Jolly and C. Xiong (1995), *On computing the long-time solution of the 2D Navier-Stokes equations*, Theoret. Comp. Fluid Dynamics, **7**, 261.

[25] D.A. Jones, L.G. Margolin and E.S. Titi (1995), *On the effectiveness of the approximate inertial manifold - a computational study*, Theoret. Comp. Fluid Dynamics, **7**, 241 .

[26] A. Debussche, T. Dubois and R. Temam (1995), *The nonlinear Galerkin method: A multi-scale method applied to the simulation of homogeneous turbulent flows*, Theoret. Comp. Fluid Dynamics, **7**, 279.

[27] Special issue on : *Inertial manifolds and their application to the simulation of turbulence*, R. Temam, Guest Editor, Theoret. Comp. Fluid Dynamics, **7** (1995).

[28] M. Hossain (1991), *Non-diffusive subgrid modeling of turbulence*, Physics Letters A, **161**, 277-282.

[29] C.E. Leith and R.H. Kraichnan (1972), *Predictability of turbulent flows*, J. Atmos. Sci., **29**, 1041-1058.

[30] Y. Zhou (1993), *Degrees of locality of energy transfer in the inertial range,* Phys. Fluids A, **5**, 1092.

[31] Y. Zhou (1993), *Interacting scales and energy transfer in isotropic turbulence,* Phys. Fluids A, **5**, 2511.

[32] Y. Zhou, P.K. Yeung and J.G. Brasseur (1995), *Scale disparity and spectral transfer in anisotropic numerical turbulence* Phys. Rev. E (in press).

[33] J. Jimenez, A.A. Wray, P.G. Saffman and R.S. Rogallo (1993), *The structure of intense vorticity in isotropic turbulence*, J. Fluid Mech., **255**, 65-90.

[34] A.A. Townsend (1976), *The structure of turbulent shear flows*, Cambridge University Press.

[35] J.C.R. Hunt (1978), A review of the theory of rapidly distorted turbulent flows and its applications, *Fluid Dyn. Trans.*, **9**, 121.

[36] W.C. Reynolds (1987), Fundamentals of turbulence for turbulence modeling and sim ulations, Lecture Notes for Von Karman Institute.

Figure 1a: Energy and enstrophy spectra at $T = 13.5\tau$ (intermediate time) for the simulation S_1.

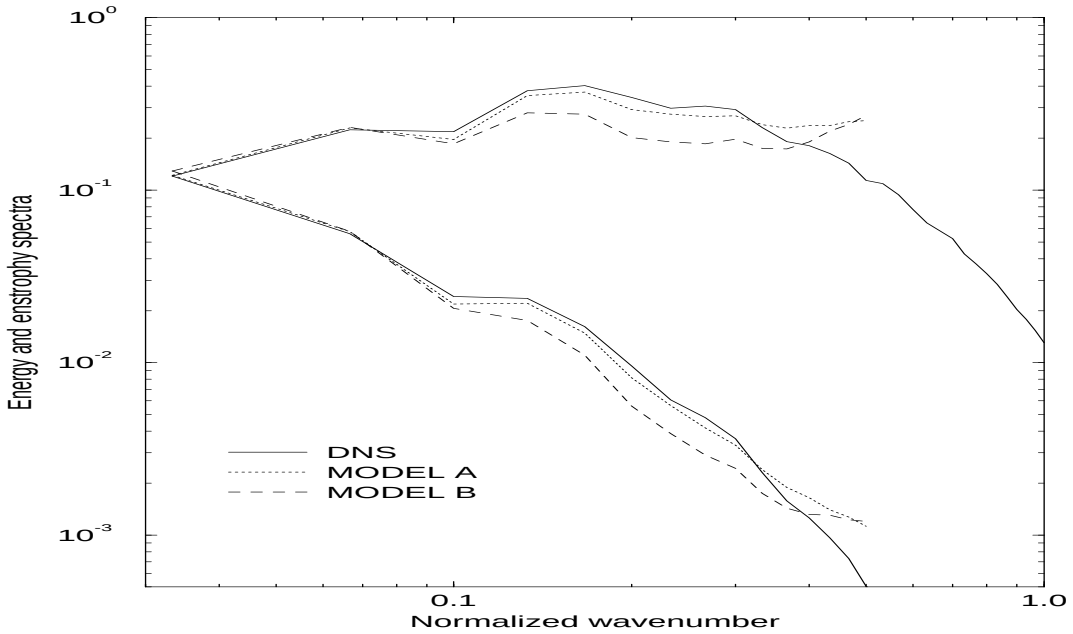

Figure 1b: Energy and enstrophy spectra at $T = 27\tau$ (final stage of the time integration) for the simulation S_1. The normalized wavenumber is defined as k/k_η, where k_η is the Kolmogorov wavenumber.

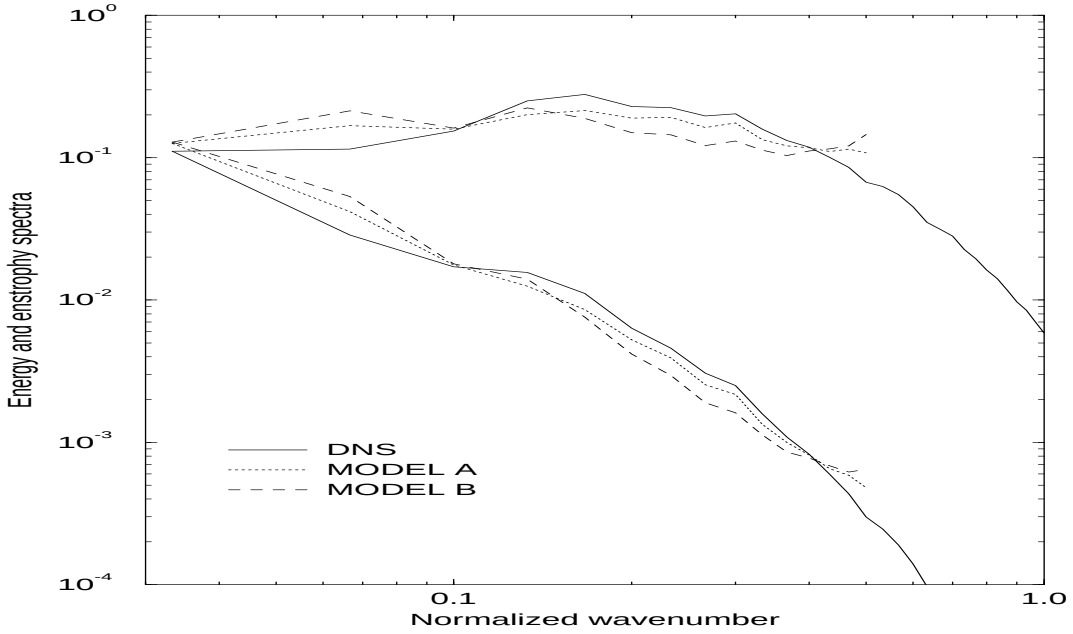

Figure 1c: Energy and enstrophy spectra at $t = 6\tau$ (intermediate time) for the simulation S_2.

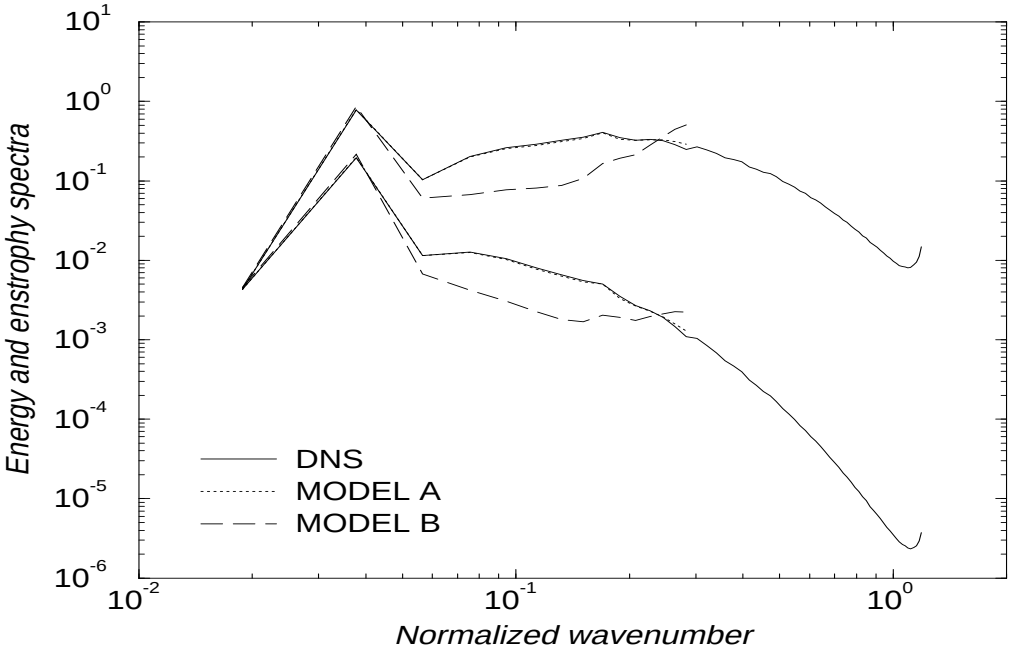

Figure 1d: Energy and enstrophy spectra at $T = 12\tau$ (final stage of the time integration) for the simulation S_2.

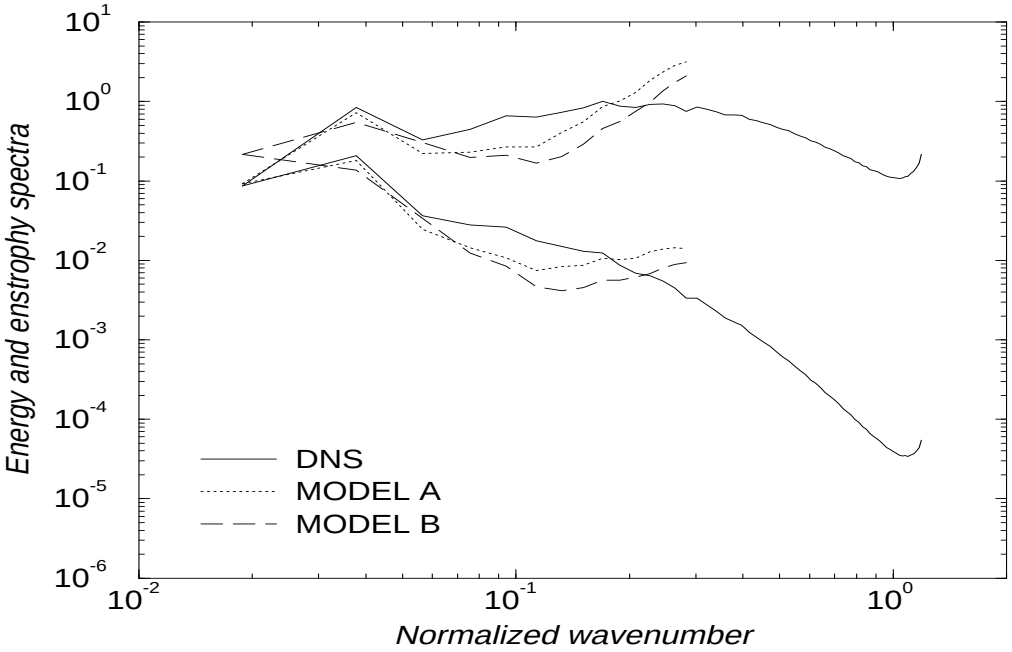

Figure 2a: Normalized averaged kinetic energy spectra $\varepsilon_r^{-\frac{2}{3}} k^{\frac{5}{3}} E(k)$ for the simulation S_1, where ε_r is the energy dissipation rate.

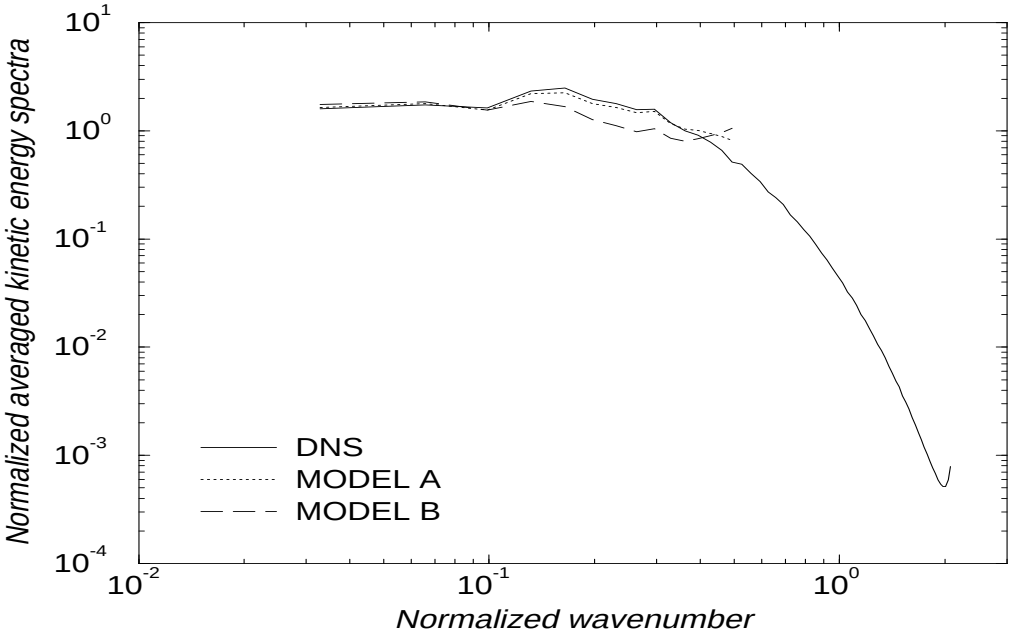

Figure 2b: Normalized averaged kinetic energy spectra $\varepsilon_r^{-\frac{2}{3}} k^{\frac{5}{3}} E(k)$, for the simulation S_2.

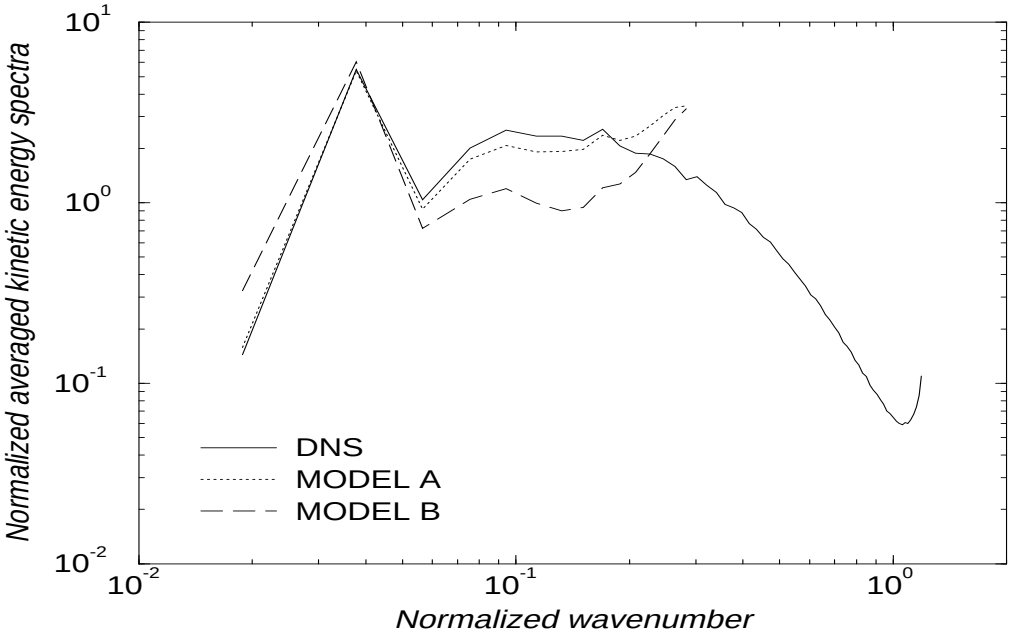

Figure 3a: Time evolution of the skewness factor of the velocity derivative $F_3(\frac{\partial u_1}{\partial x_1})$ for the simulation S_1. From Figures 3-6 the time is in units of an eddy turnover time.

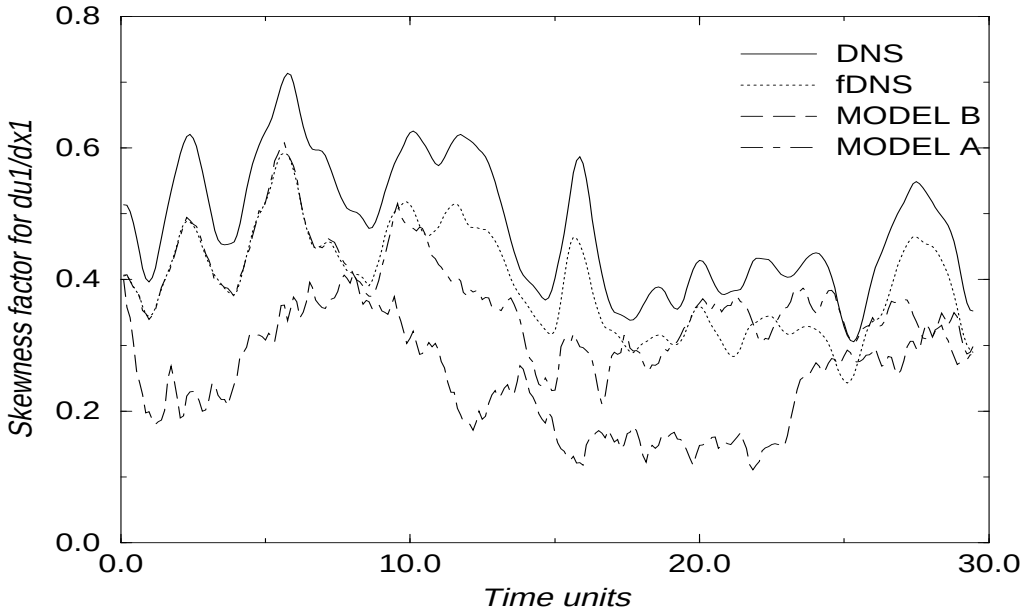

Figure 3b: Time evolution of the skewness factor of the velocity derivative $F_3(\frac{\partial u_1}{\partial x_1})$ for the simulation S_2.

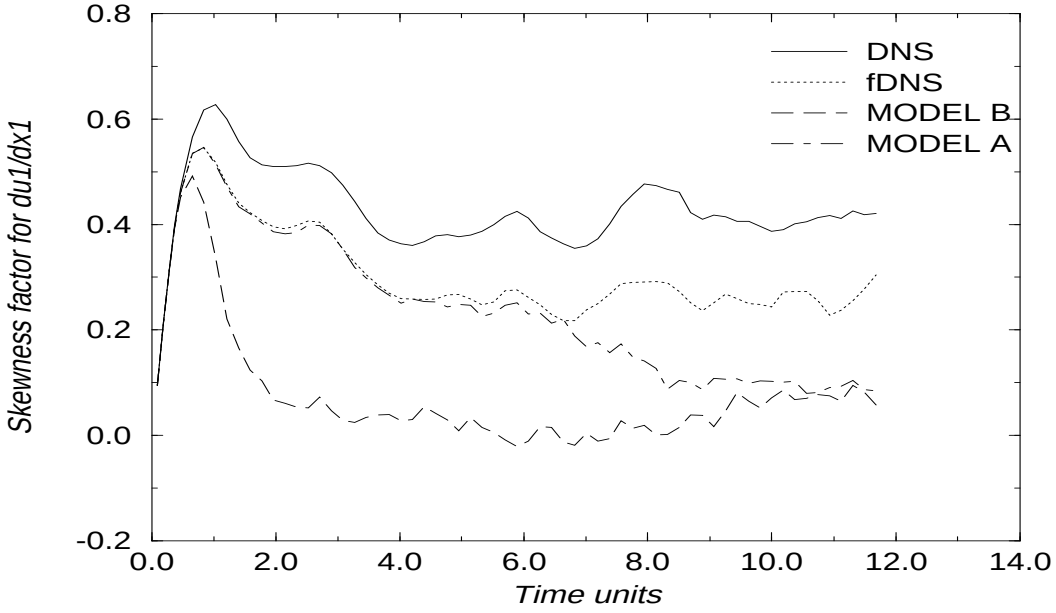

Figure 4a: Time evolution of the flatness factor of the velocity derivative $F_4(\frac{\partial u_1}{\partial x_1})$ for the simulation S_1.

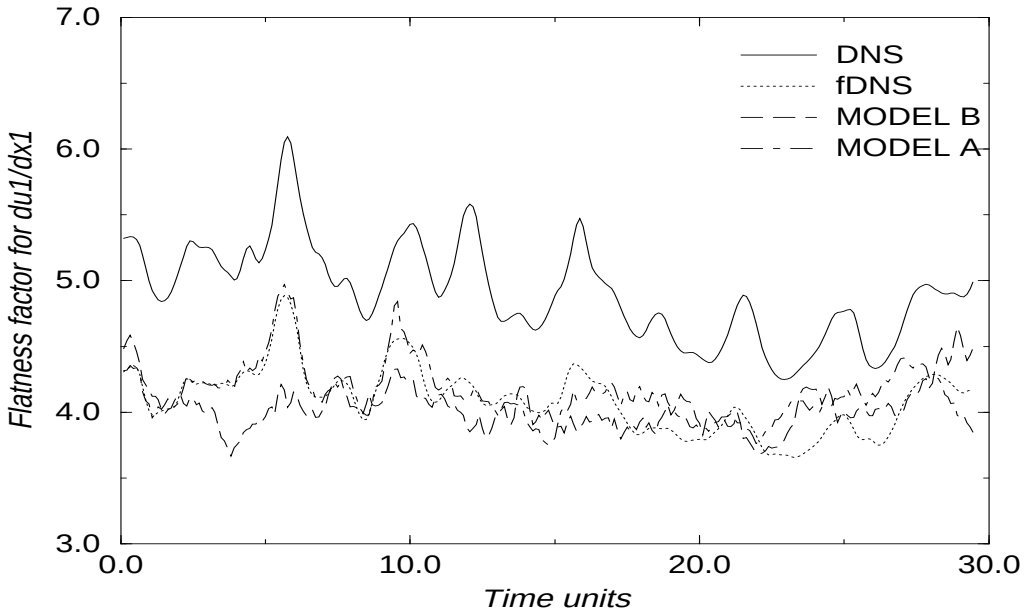

Figure 4b: Time evolution of the flatness factor of the velocity derivative $F_4(\frac{\partial u_1}{\partial x_1})$ for the simulation S_2.

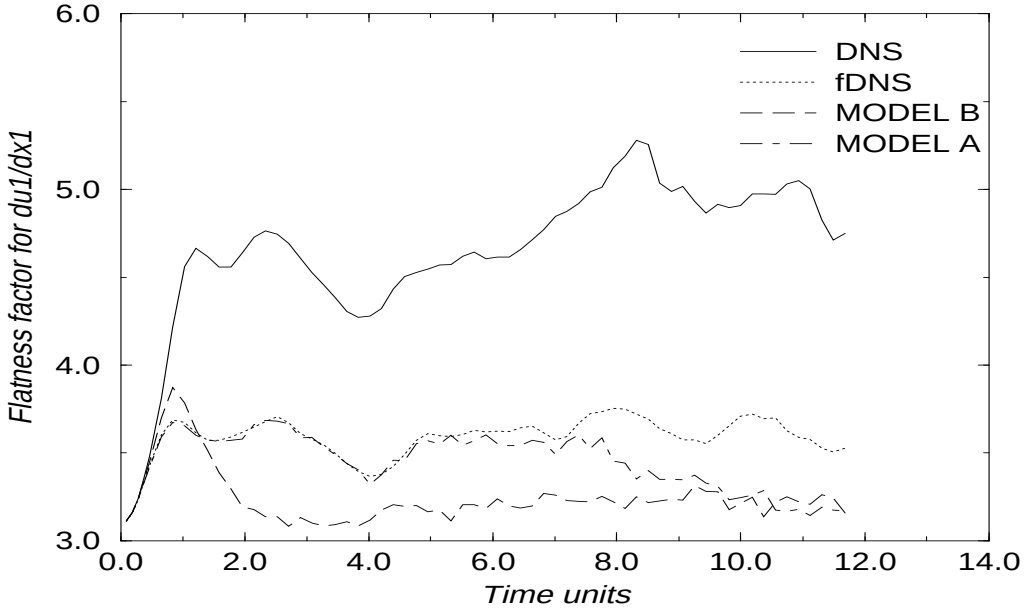

Figure 5a: Time evolution of the flatness factor of the velocity $F_4(u_1)$ for the simulation S_1.

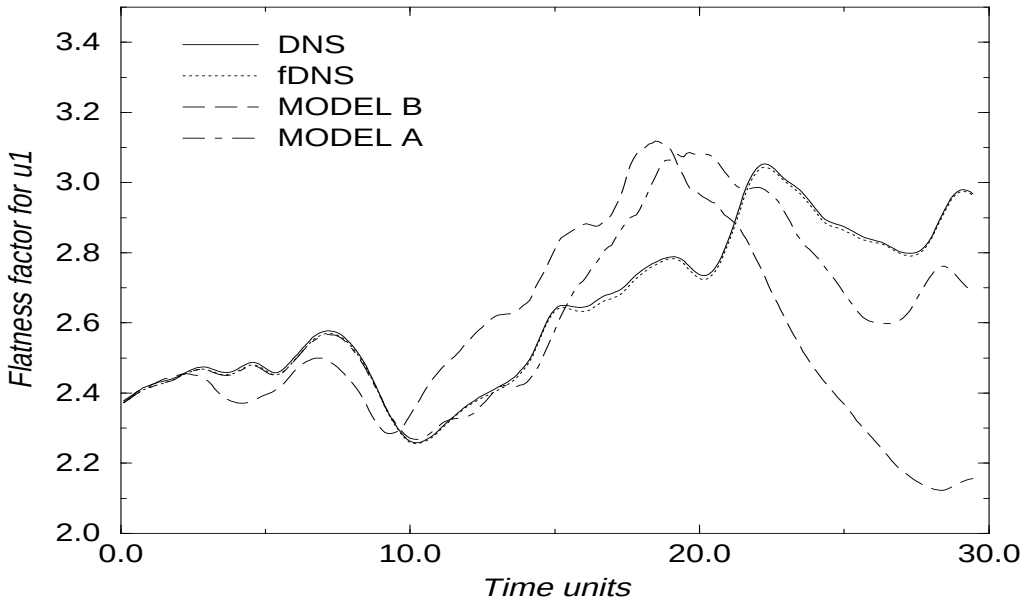

Figure 5b: Time evolution of the flatness factor of the velocity $F_4(u_1)$ for the simulation S_2.

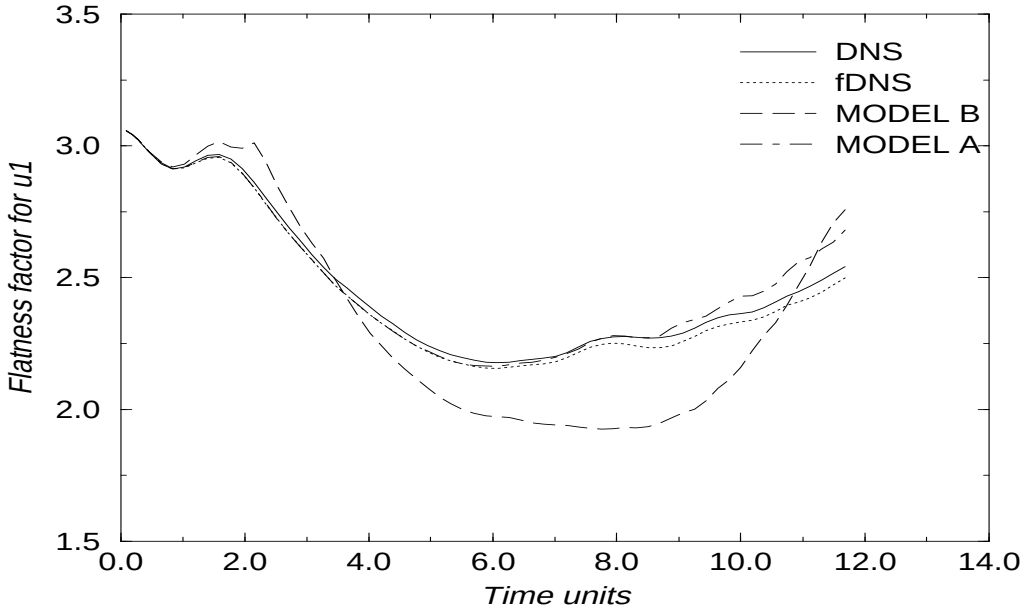

Figure 6: Time evolution of the correlation coefficient Γ for the simulation S_1.